



## RESEARCH ARTICLE

10.1029/2020JD032683

### Key Points:

- Cloud microphysical properties were retrieved from a geostationary satellite
- These properties were accessed by geostationary and polar orbits satellites and in situ radiosonde observations in complex cloud region
- Retrieved cloud information from Himawari-8/AHI agreed with passive and active sensor and in situ radiosonde data

### Correspondence to:

C.-Y. Liu,  
cylui@g.ncu.edu.tw

### Citation:

Liu, C.-Y., Chiu, C.-H., Lin, P.-H., & Min, M. (2020). Comparison of cloud-top property retrievals from Advanced Himawari Imager, MODIS, CloudSat/CPR, CALIPSO/CALIOP, and radiosonde. *Journal of Geophysical Research: Atmospheres*, 125, e2020JD032683. <https://doi.org/10.1029/2020JD032683>

Received 2 MAR 2020

Accepted 15 JUN 2020

Accepted article online 22 JUN 2020

### Author Contributions:

**Conceptualization:** Chian-Yi Liu

**Formal analysis:** Chi-Hao Chiu, Po-Hsiung Lin, Min Min

**Funding acquisition:** Chian-Yi Liu

**Investigation:** Chian-Yi Liu

**Methodology:** Chian-Yi Liu, Po-Hsiung Lin, Min Min

**Project administration:** Chian-Yi Liu

**Resources:** Chian-Yi Liu

**Software:** Chi-Hao Chiu, Min Min


**Validation:** Chi-Hao Chiu

**Visualization:** Chi-Hao Chiu

**Writing - original draft:** Chian-Yi Liu

**Writing - review & editing:** Chian-Yi Liu, Po-Hsiung Lin, Min Min

## Comparison of Cloud-Top Property Retrievals From Advanced Himawari Imager, MODIS, CloudSat/CPR, CALIPSO/CALIOP, and Radiosonde

Chian-Yi Liu<sup>1,2</sup> , Chi-Hao Chiu<sup>2</sup>, Po-Hsiung Lin<sup>3</sup>, and Min Min<sup>4</sup>

<sup>1</sup>Center for Space and Remote Sensing Research, National Central University, Taoyuan, Taiwan, <sup>2</sup>Department of Atmospheric Sciences, National Central University, Taoyuan, Taiwan, <sup>3</sup>Department of Atmospheric Sciences, National Taiwan University, Taipei, Taiwan, <sup>4</sup>School of Atmospheric Sciences and Guangdong Province Key Laboratory for Climate Change and Natural Disaster Studies, Sun Yat-sen University, Zhuhai, China

**Abstract** The information on cloud properties and microphysical characteristics is critical for environmental research and application, such as that on weather, climate, hydrology, and green energy and Earth energy budget. The launch of the new-generation geostationary satellite, for example, the Japanese Himawari-8, enables retrieval of cloud information through multichannel observation. To confirm the retrievals from the Advanced Himawari Imager (AHI) onboard Himawari-8 (Himawari-8/AHI), this study accessed the cloud retrievals from AHI and compare them against those obtained from spaceborne passive and active sensors on the low Earth orbit satellites, such as NASA's CloudSat, Cloud-Aerosol Lidar and Infrared Pathfinder Satellite Observations (CALIPSO). The atmospheric thermodynamic state from in situ radiosonde provides another dimension for evaluating the retrieved cloud-top temperature and height, which were obtained and analyzed during two research cruises over the South China Sea during monsoon onset season with large cloud variability to ensure the comprehensive intercomparisons. The findings show that the cloud-top altitude, cloud optical thickness, and cloud effective particle radius retrieved from AHI are consistent with passive Moderate Resolution Imaging Spectroradiometer (MODIS) data. Furthermore, both spaceborne active Cloud Profiling Radar (CPR) and Cloud-Aerosol Lidar with Orthogonal Polarization (CALIOP) data confirm the low uncertainty of cloud-top altitude, particularly when the cloud is optically thick. Large cloud-top altitude discrepancy among these data in the optically thin cloud might be due to the limited AHI spectral channels or instrumental spatial resolutions. The cloud-top temperature and altitudes in either liquid or ice phase cloud agree well with collocated sounding profiles, with low difference of 1 K and 170 m, respectively.

## 1. Introduction

Clouds play a unique and crucial role in Earth climate and environment because of their strong influence on incident solar and outgoing thermal radiation. Furthermore, extreme weather such as storm or heavy precipitation can be associated with specific cloud microphysical processes, and hence, knowledge of cloud-top properties is essential for nowcasting and warning. For example, cloud-top height (CTH) is the upper boundary in altitude where atmospheric moisture condenses into cloud particles during a fair weather, and cloud optical thickness (COT) might affect both downward solar and upward terrestrial radiation. Change in either CTH or COT will lead to the modification of the Earth energy budget (Stephens et al., 1990). Therefore, understanding the cloud microphysics is crucial for phenomenon interpretation, mechanism analysis, model simulation, and scale verification (Bayler et al., 2000).

Because of cloud complexity, satellite observation for advanced, cloud-related derived products must be conducted through multichannel and high-spectral resolution observation, which is being implemented since late 1970s and 1990s, respectively. Cloud properties obtained using instruments onboard a spaceborne platform, in particular on low Earth orbit, were used to investigate the differences. Coakley and Bretherton (1982) and Molnar and Coakley (1985) use multichannel observation to detect cloud layers and apply a statistically equivalent spatial coherence (SESC) formula to detect two-layered cloud system and its horizontal coverage. Ackerman et al. (1998) and Menzel et al. (2016) have applied High-resolution Infrared Radiation Sounder (HIRS) observation to derive the cloud-top pressure (CTP)

©2020. The Authors.

This is an open access article under the terms of the Creative Commons Attribution-NonCommercial-NoDerivs License, which permits use and distribution in any medium, provided the original work is properly cited, the use is non-commercial and no modifications or adaptations are made.

and COT and address the uncertainties with spectral sensitivity and variability. Li et al. (2001) and Li, Huang, et al. (2005) used both 1DVAR and minimum residual algorithms to determine cloud microphysical properties from high-spectral resolution Atmospheric Infrared Sounder onboard National Aeronautics and Space Administration's (NASA's) Aqua satellite. Weisz et al. (2007) and Yao et al. (2013) conducted a detailed comparison for the CTH retrievals between a passive sensor, such as Moderate Resolution Imaging Spectroradiometer (MODIS), and an active radar/lidar instrument, such as Cloud Profiling Radar (CPR) onboard CloudSat and Cloud-Aerosol LIDAR with Orthogonal Polarization (CALIOP) onboard Cloud-Aerosol Lidar and Infrared Pathfinder Satellite Observation (CALIPSO). The CTH retrievals obtained from polar-orbiting satellites are in agreement with a root-mean-square difference, and bias of approximately 2 and  $-1$  km was noted from the synthetic analysis of passive and active observation, respectively.

The cloud information obtained from a geostationary orbit can be used to analyze and monitor its relationship to extreme weather. For example, Hamada and Takayabu (2016) estimated the convective cloud-top vertical velocity from the decreasing rate of infrared (IR) brightness temperature (BT) over the south of Japan through rapid scan observation in boreal summer. Kobayashi and Masuda (2008) indicated the relationship between COT and cloud particle size associated with precipitation. Bedka et al. (2015) also suggest that rapid cooling in the cloud-top temperature (CTT) and increase in CTH are typically followed by severe hail and damaging gust wind at the ground level. These confirmed the potential links between cloud properties along with microphysics parameters and the high impact weather or climate studies. Therefore, obtaining cloud information from a geostationary orbit might maximize the benefit to these studies.

Since the launch of the Japanese weather satellite Himawari-8 in October 2014 and its operation from July 2015, the Advanced Himawari Imager (AHI) is the primary payload on this geostationary satellite, and it has a 16-channel multispectral imager for capturing images from visible to IR bands over the Asia-Pacific region (Bessho et al., 2016). The AHI has spectral and spatial characteristics similar to Advanced Baseline Imager (ABI) (Schmit et al., 2005), Advanced Meteorological Imager (AMI), Advanced Geostationary Radiation Imager (AGRI) on the U.S.'s GOES-16 (Geostationary Operational Environmental Satellite-16), Korea's GEO-KOMPSAT-2A (Geostationary Korea Multi-Purpose Satellite-2A), and China's Feng-Yun-4A, respectively. The AHI can observe with resolutions of 500 m ( $0.64\ \mu\text{m}$ ), 1 km ( $0.47\text{--}0.51\ \mu\text{m}$ ) to 2 km ( $1.6\text{--}13.3\ \mu\text{m}$ ) full-disk coverage at every 10 min in its regular mode. These channels are designed to observe the Earth's surface, atmospheric moisture, clouds from the shortwave reflectance, and longwave radiances. Therefore, associated atmospheric thermodynamic state, clouds, and surface properties can be inferred from multichannel observation. Community Satellite Processing Package for geostationary satellite (CSPP-GEO) package has been developed at the Cooperative Institute for Meteorological Satellite Studies (CIMSS) at University of Wisconsin-Madison and is able to provide not only calibrated and geolocated sensor observation but also cloud retrievals from raw satellite telemetry (Martin et al., 2016) as a research algorithm. With the localized lookup tables (LUTs) for AHI's spectral bands and the use of high-resolution atmospheric thermodynamic states (Liu, Kuo, et al., 2016) at 3-km horizontal grid resolution, the cloud products are inferred from ABI with CSPP-GEO and hereafter referred to as AHI retrieval. The retrieval is a result of sophisticated procedure, based on calculation of Planck thermal radiation LUTs for pixel by pixel of latitudes, longitudes, sensor azimuth/zenith angles, land/sea mask, and ecosystem type for surface IR emissivity/shortwave albedo as well as elevation. A Pressure layer Fast Algorithm for Atmospheric Transmittances model (Eyre & Woolf, 1988) had been modified by CIMSS to compute clear-sky atmospheric radiances and transmittances for AHI's IR bands from atmospheric thermodynamic states at a given pixel. Hence, observed and calculated radiances are used in the retrievals of cloud properties (Li et al., 2001; Li, Liu, et al., 2005; Liu et al., 2008; Yao et al., 2013) through one-dimensional variational (1DVAR) technique. The retrieved science products were mainly focused on cloud phase, cloud-top features, cloud effective particle radius, cloud ice water path, and so on (Heidinger et al., 2012; Liu et al., 2012; Menzel et al., 2008; Strabala et al., 1994).

The primary objective of this study was to assess the performance of cloud retrievals from AHI onboard Himawari-8 (Himawari-8/AHI) observation by using CSPP-GEO. Although similar studies had been conducted (e.g., Huo et al., 2020; Lai et al., 2019; Letu et al., 2019; Tan et al., 2019), the cloud properties have not been comprehensively evaluated with either active or passive instrument (e.g., CPR, CALIOP, or MODIS) in an unstable atmospheric condition. In particular, the variability and bias of AHI cloud properties will be quantified as a function of cloud phases, CTH, and COT, which will lead to improved utilization of

AHI radiances such as the assimilation of cloudy radiances in numerical weather prediction models. Moreover, CTT and moisture information are compared with data from radiosonde soundings so that the clouds are analyzed not only for their microphysical properties but also thermodynamic state.

Section 2 describes the data and method adopted in this study. The comparison and evaluation of data are discussed in section 3. Finally, conclusions are summarized in section 4.

## 2. Data

While Himawari-8/AHI in the geostationary orbit was primarily designed to provide new capacity levels for identifying and tracking rapidly changing weather phenomena and derive quantitative products for the weather and climate application (Bessho et al., 2016), it also represents a big contribution for research. AHI has a higher radiometric, spectral, and spatial resolution than what was available on previous radiometers in the geostationary orbit. Similar instruments, such as ABI, AMI, and AGRI, enable retrieval of cloud information, motion vectors, and associated environmental parameters as well (Greenwald et al., 2016; Martin, 2007; Schmit et al., 2005). Navigated and calibrated reflectance and radiance in Level 1, along with AHI cloud products in Level 2, are obtained and retrieved using CSPP-GEO.

To evaluate cloud products from a geostationary orbit, the cloud products retrieved from MODIS are used as reference. MODIS is a radiometer onboard the NASA Terra and Aqua polar-orbiting platforms and has 36 spectral bands whose wavelengths range from 0.4 to 14.4  $\mu\text{m}$ . With 2,330-km swath from approximately 700-km orbital altitude, MODIS achieves global coverage every 1–2 days (King et al., 1992). In this study, the operational MODIS Level 2 cloud products from Standard Collection 6.1 (MOD06/MYD06) (Platnick et al., 2003) with 5-km spatial resolutions are used.

In addition to passive MODIS cloud products, cloud properties from active radar, the CPR, are used as well. The CPR on CloudSat is a 94-GHz nadir-looking active radar, which measures the energy backscattered by both clouds and precipitation within 1.7 along track by 1.4 across-track radar footprint (Stephens et al., 2009). The CloudSat/CPR can penetrate all nonprecipitating clouds but has low sensitivity to thin cirrus, particularly those with small ice particle size. Extended cloud boundaries can be resolved at every 240 m vertically for up to 125 layers from the ground.

Spaceborne active lidar is sensitive to clouds, in particular thin cirrus and aerosols, owing to its optical wavelength. Cloud-Aerosol Lidar with Orthogonal Polarization (CALIOP) on CALIPSO can provide measurements at 0.532 and 1.064  $\mu\text{m}$ , which are used to obtain the vertical structure of clouds and aerosols as its designed mission (Winker et al., 2007). CALIPSO/CALIOP provides information regarding layers down to the level in which the lidar signal is fully attenuated even in the case of multilayer clouds. In this study, spatial resolution of 5 km in the Level 2 cloud layer information (Version 3) is used to identify the existence of cloud and its altitude information in a confidence. The highest altitude of the cloud was used in this study, although CALIOP provided the cloud layer top altitudes in the case of multilayer clouds.

For comparing cloud properties obtained from various instruments onboard multiple platforms, analysis for a large variability of clouds must be conducted in complex types, in terms of CTHs from low to high, optically thin to thick, scattered cloud coverage to overcast within single-pixel instantaneous field of view, and cloud phases from liquid warm water stratus to solid cold ice convective clouds. Therefore, the comprehensive cloud microphysics properties, during the East Asian summer onset (EASMO) period over the South China Sea (SCS), provide a great opportunity for the purpose of this study because of extremely unstable atmospheric dynamic and thermodynamic conditions. Moreover, the retrieval of cloud properties might presence the biases that correlate to sensor's view angle (Várnai & Marshak, 2007). The sensor's scan angles in this region of Himawari-8/AHI are from 35° to 45°, which are comparable with the MODIS maximum scan angle. Thus, several types of clouds with complex structures under similar sensors' scan scenes are suitable for this assessment study.

We retrieved the cloud products from 21 to 25 May 2016, over the latitudes of 5°S to 30°N and longitudes of 105–130°E following the definition of EASMO by B. Wang et al. (2004). Identical cloud retrievals were performed during two field campaigns in December of 2016 and 2017 for additional intercomparisons to the radiosonde soundings as well. All AHI cloud products were retrieved at its original 2-km spatial resolution and resampled to 5-km spatial resolution to fit MODIS cloud product. As some of the cloud properties are



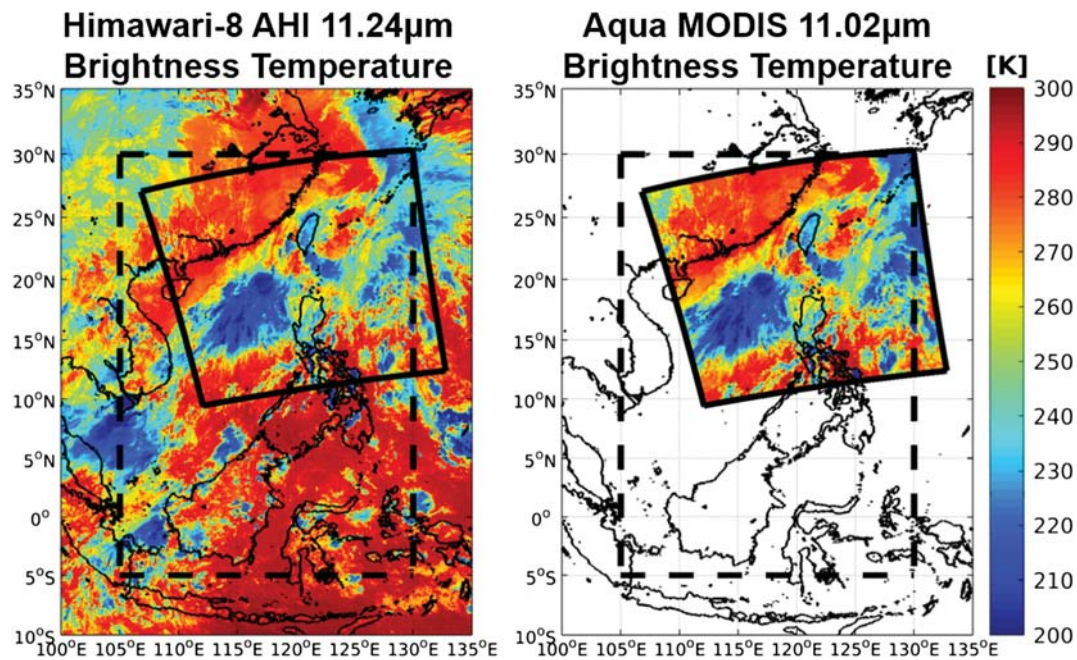


**Figure 1.** Comparison of Himawari-8 (left panel) and Aqua/MODIS (right panel) IR window channel brightness temperature at 0520Z 22 May 2016: (left panel) AHI band 14 (11.24  $\mu\text{m}$ ) brightness temperature; (right panel) MODIS band 31 (11.02  $\mu\text{m}$ ) brightness temperature.

based on shortwave channel measurement, such as COT and cloud effective particle radius (CDe), the comparisons are performed during daytime only.

In addition to the spaceborne instrumental data set, in situ observation from traditional radiosonde might provide an additional dimension to evaluate the cloud property retrieval. Owing to the measured physical quantity of radiosonde, the atmospheric temperature and moisture along with sensor's geographical information (e.g., latitude, longitude, and altitude) are transmitted back to the receiver immediately during the drifting and ascending of the balloon. Therefore, using a precise spatial and temporal collocation procedure, considering location and altitude against each individual cloud retrieval from Himawari-8/AHI observation, the CTH and CTT could be evaluated from the radiosonde measurement. During the SCS Two-Island Monsoon Experiment (SCSTIMX) from 2016 to 2019, data from two cruises of Research Vessel Ocean Research 1 (R/V OR1) were used, namely, 11–21 December 2016 and 3–21 December 2017 (Sui et al., 2020). The Vaisala MW41 sounding receiver acquires and processes the Vaisala RS41 radio signal to obtain atmospheric soundings during these two R/V cruises, twice (00 and 12Z) per day and up to four times (00, 06, 12, and 18Z) when intense observation is needed.

### 3. Comparison and Evaluation Analysis

Although Himawari-8/AHI is an onboard geostationary satellite that enables 24-hr continuous full-disk observation at 10-min interval, CloudSat/CPR, CALIPSO/CALIOP, and Aqua/MODIS are polar-orbiting satellites, and each orbital swath covers only a limited area within the Himawari-8/AHI full-disk imagery. Therefore, a spatiotemporal collocation procedure was performed to ensure the observation and retrieved cloud parameters from different platforms are comparable in the close spatial regions and temporal windows. This resulted in five MODIS data granules, at 0610Z, 0520Z, 0600Z, 0640Z, and 0550Z, on each individual day from 21 to 25 May 2016 within the target domain for the following analysis. Figure 1 shows the example for MODIS and AHI observations at bands 31 (11.02  $\mu\text{m}$ ) and 14 (11.24  $\mu\text{m}$ ) at 0550Z 25 May 2016, respectively. We could identify a developing deep convective system in the center of SCS and west vicinities of Luzon Island in the Philippine that the system had a very low BTs. Associate COT, CDe, and CTH are shown in Figure 2. An agreement was observed not only in spatial patterns but also in the magnitudes of either IR window channel BTs or retrieved COT (Figures 1 and 2). However, products based on AHI data exhibit larger cloud coverage, in particular, over the northern SCS. This is because not only the MODIS

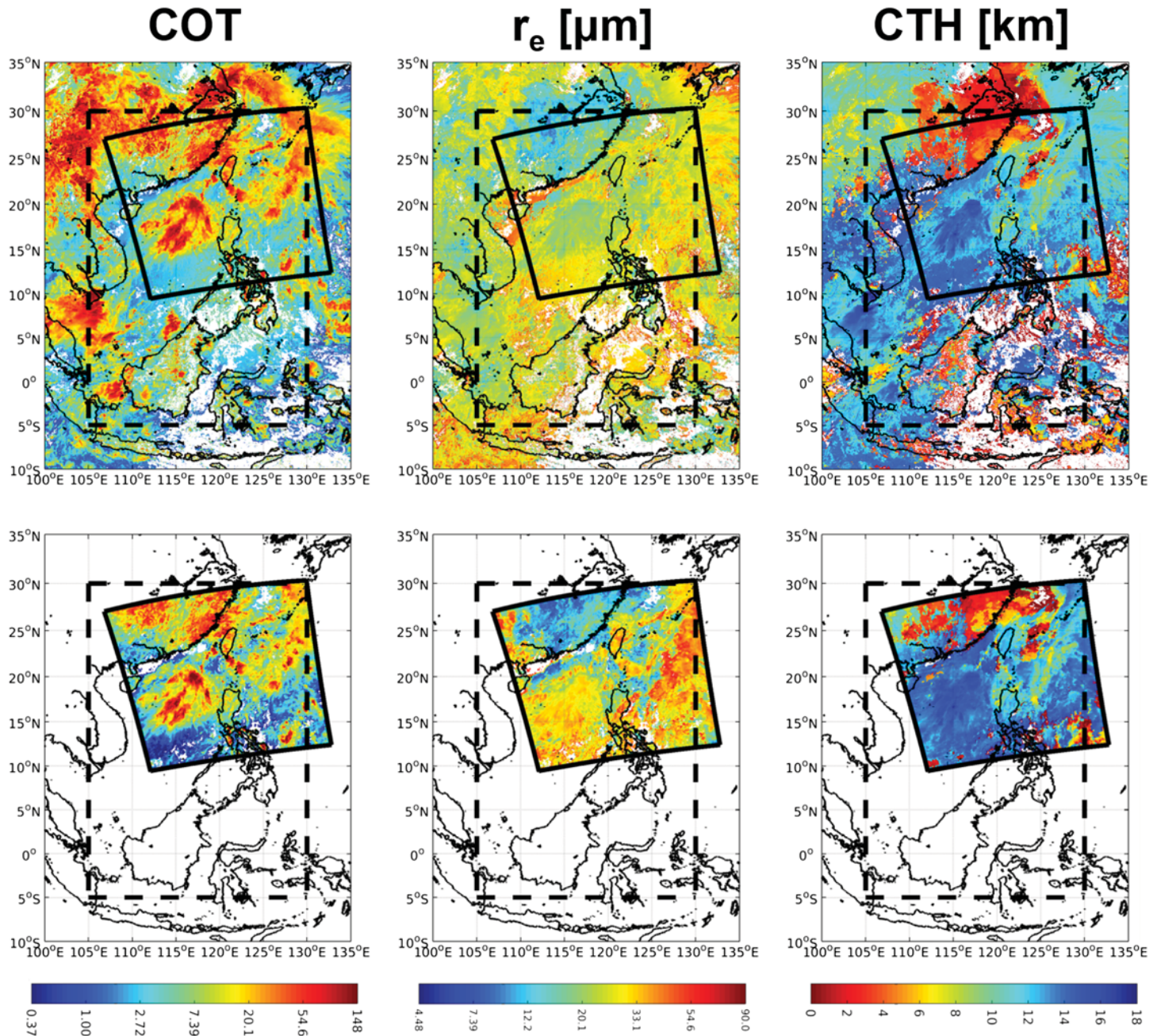


**Figure 2.** Comparison of Himawari-8 and operational Aqua/MODIS (MYD06) retrieved COT (left column), CDe (middle column), and CTH (right column) at 0520Z 22 May 2016. The panels in the top (bottom) row are the retrievals from AHI (MODIS) observation.

has higher spatial resolution in shortwave channels than AHI has but also the AHI instrument has coarser resolution than MODIS; thus, the chances of having the cloud in the field of view are higher.

We analyzed the COT and CDe retrieval differences between AHI and MODIS in five consecutive days during 21–25 May 2016, and the result are shown in Figures 3 and 4 as the probability distribution function curves. Figure 3 indicates the COT from AHI is slightly larger than that from MODIS among all clouds (black curve) because the discrepancy histogram is centered slightly greater than 0 with the standard deviation (STDE) < 3. Ice phase cloud (red curve) dominates the major sample because it shows higher probability than water phase cloud (blue curve). The STDEs of three cloud phases are all lower than 3 and reveal that both AHI and MODIS COT are highly correlated with each other. This can be verified from the bars with



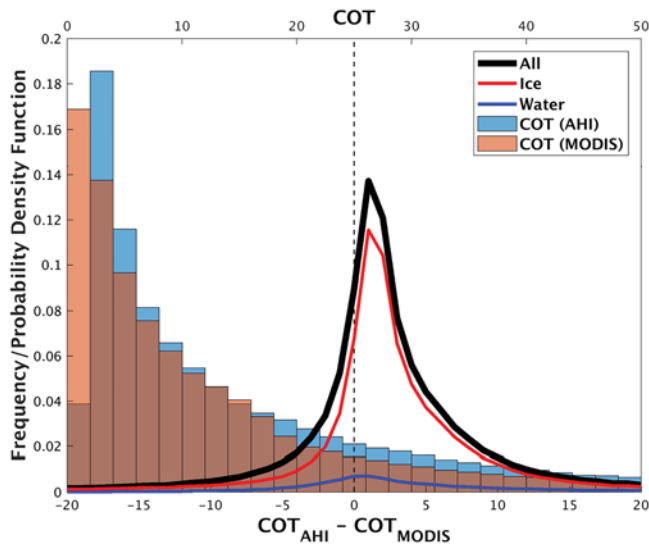


**Figure 3.** Histogram of COT retrieval difference between AHI and MODIS for all cloud (black curve), ice phase cloud (red curve), water phase cloud (blue curve), and cloud with undertrain phase (pink curve). Bars indicate the occurrence frequency for AHI and MODIS at 2.5  $\mu\text{m}$  incrimination of COT bins, which is labeled on the top x axis.

tions. The cloud properties from other platforms must be analyzed to quantify the discrepancy of the retrieved cloud properties.

We performed a synthetic CTH analysis using passive sensors (i.e., AHI and MODIS) as well as active instruments (i.e., CALIOP and CPR; Figure 5). Pixels along the CALIOP/CPR ground track that were covered by AHI (0550Z) and three granules MODIS granules (from 0545 to 0555Z) CTH retrievals on 25 May 2016 were investigated. Table 1 lists the mean difference (bias) and the STDE of the differences between the CTH obtained using the given instruments. The highest level of CPR L2 Cloud Mask product was a cloud mask

value  $>30$  (high confidence in the cloud detection) (Sohn et al., 2015; Yao et al., 2013), and the first layer on top of CALIOP cloud product was defined as CPR and CALIOP CTH. In general, the CTH retrieved from AHI and MODIS agrees well along with the tracks of CloudSat and CALIPSO vertical profiles, and these retrievals are closer to the values from CPR than from CALIOP. Mean differences of AHI CTH with respect to CPR and CALIOP are smaller than MODIS CTH product.

The vertical cross section along the CloudSat/CALIPSO ground track is shown in Figure 5b. CloudSat L1 CPR reflectivity in dBZ (in colorscale) is overlaid with CTHs in kilometers from AHI (pink triangles), MODIS (green diamonds), CPR (blue dots), and CALIOP (orange stars). It illustrates the difference between the lidar and radar instruments in characterizing clouds. Lidar is highly sensitive to ice crystals in optically thin cloud and therefore detects high cloud-top altitudes (e.g., between latitudes  $0^\circ\text{N}$  and  $17^\circ\text{N}$ ). By contrast, radar is unable to measure optically thin clouds but receives reflectivity from large cloud particles. Thus, CTHs from the radar are lower than from the lidar (Figure 5b). Synthetic observations from both lidar and radar could provide a better description of cloud vertical structure and extent.

IR sensitivity of optically thick clouds is better than that of thin clouds owing to large differences between cloudy and clear radiances for CTP retrievals. Thus, the agreement between AHI and MODIS CTH is good for thick and high clouds with strong radar reflectivity from latitudes  $7^\circ\text{N}$  to

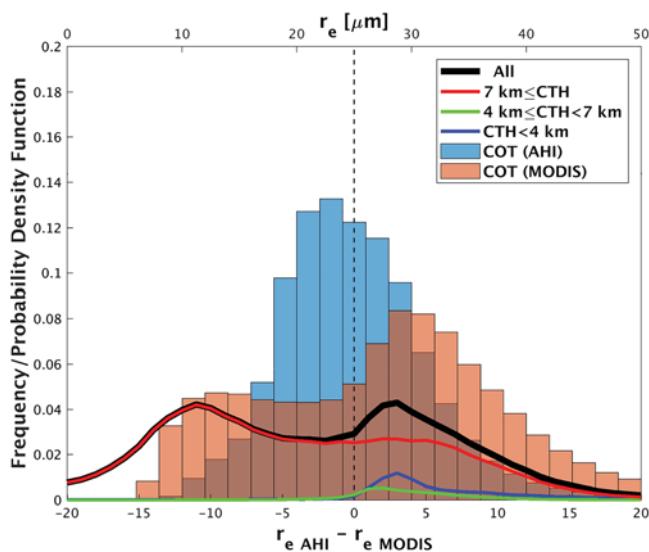


**Figure 4.** Histogram of CDe retrieval difference between AHI and MODIS for all cloud (black curve), high cloud (red curve), middle cloud (green curve), and low cloud (blue curve). Bars indicate the occurrence frequency for AHI and MODIS at 2.5- $\mu\text{m}$  incrimination of CDe bins, which is labeled on the top x axis.

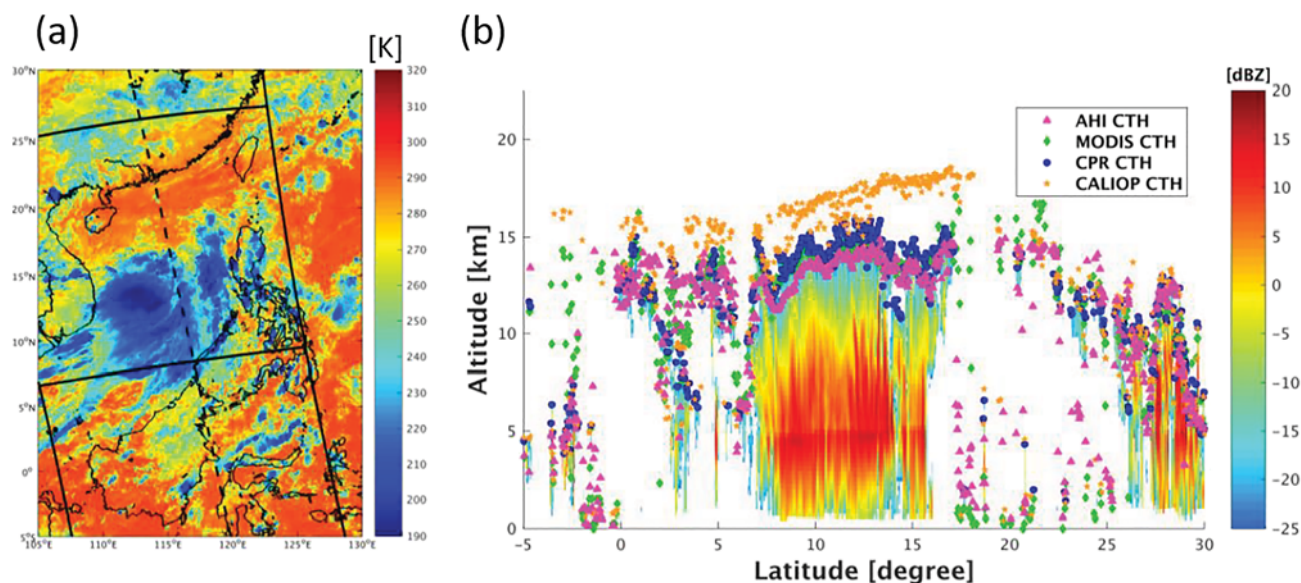


**Figure 5.** (a) The brightness temperature in kelvins for AHI band 14 (11.2 μm) at 0550Z on 25 May 2016, with outlines of three MODIS granules (black) (viz., 0545Z, 0550Z, and 0555Z from south to north), and CloudSat/CALIPSO track (black dash line). (b) AHI retrieved CTH and operational MODIS CTH (MYD06) along with CPR; CALIOP CTH products are shown in (a) as indicated in the legend at the top right corner. Color shading indicates CloudSat/CPR reflectivity in dBZ. The cloud-top heights from AHI, MODIS, CPR, and CALIOP are represented as magenta triangles, green diamonds, blue dots, and orange pentagrams, respectively.

15°N and 26°N to 30°N. The area in-between (i.e., from latitudes 7°N to 15°N) the lidar retrieves high altitudes of cirrus, which the radar does not observe. MODIS CTH occasionally has extreme values (e.g., latitudes from 18°N to 23°N for close-to-surface or higher-than-lidar CTH) might due to coarser spatial resolution of the used atmospheric thermodynamic state in MODIS retrieval. Overall, AHI CTHs are closely parallel to the radar CTH. Results from MODIS are similar, although in some areas, MODIS attempts to reach high altitudes (e.g., latitudes 4°S to 2°S) because of its high spatial resolution to observe broken clouds as lidar does.

To define the in situ atmospheric thermodynamic state of the cloud top, radiosonde could be one of the economic and accurate methods other than aircraft direct measurement. In December 2016 and 2017, two cruises conducted as part of SCSTIMX. These two winter field campaigns were designed to investigate the cloud-precipitation and large-scale dynamic processes over the SCS (Sui et al., 2020). Up to 32 and 10 radiosondes were released during 11–21 December 2016 and 1–10 December 2017, respectively (Figure 6). All the Vaisala RS41 radiosondes' drifting information while ascending were recorded by Vaisala MW41 receiver onboard Taiwan's RV/OR-1. As per the radiosonde horizontal tracks shown in Figure 7a, certain radiosonde drifts up to 100 km horizontally, and an individual radiosonde may take approximately 1 hr to travel from the surface to upper troposphere. Therefore, a spatiotemporal collocation is performed to consider the ascending and drifting of radiosonde at each scan time of the AHI data at every 10-min interval. This ensures the radiosonde is closely sampling the atmospheric thermodynamic state during ascending at collocated AHI pixel. Those soundings are collocated with AHI cloud phase as liquid and ice phases as shown in Figures 7a and 7b, respectively. The x and y axes are the sounding altitude and temperature deviations from collocated AHI CTH and CTT, respectively, where the zeros are considered the perfect match between AHI

**Table 1**  
CTH Statistics of Instrument Differences

Differences	Bias (km)	STDE (km)
AHI-CPR	−0.49	2.16
MODIS-CPR	−0.04	1.91
AHI-CALIOP	−1.96	3.82
MODIS-CALIOP	−1.51	3.02
AHI-MODIS	−0.61	2.90

CTH/CTT and sounding profiles. Figures 7a and 7b show that when the CTHs had matched the collocated radiosonde altitudes exactly, the temperature differences among soundings and CTTs are almost within 1 K. This is equivalent to a 170 and 100 m of CTH uncertainty if the temperature follows the moist and dry adiabatic lapse rate, respectively. Thus, CTT, CTH, and atmospheric thermodynamic state information may be used to estimate cloud-top emission in future.

It is also interesting to analysis the relative humidity (RH) profile in the ±200-m layer from CTH. The vertical moisture profile reveals

## The RAOB tracks of radiosondes during 2016–2017

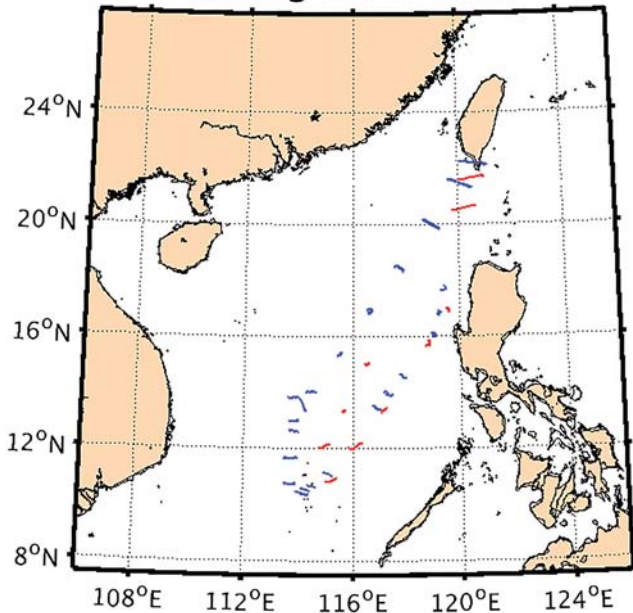


**Figure 6.** The radiosonde drifting tracks during the SCSTIMX in 2016 and 2017. The radiosondes were released from R/V OR1 during 11–21 December 2016 (blue curves) and 3–21 December 2017 (red curves).

that a relative low (high) RH when CTP is below (above) 440 hPa, while the cloud is commonly in the phase of ice (liquid). This phenomenon is shown that the ice phase cloud is in a lower RH environment than the water phase cloud, and in parallel with the finding from in situ aircraft observations (Korolev & Isaac, 2006). A decreased RH tendency was noted when the altitude was higher than collocated CTH. Thus, moisture within a cloud is more than that atop a cloud.

## 4. Summary

Using synthetic data sets on cloud properties observed or derived from passive and active instruments onboard the low Earth orbit satellites such as Aqua/MODIS, CloudSat/CPR, and CALIPSO/CALIOP, cloud information (e.g., CTH, COT, and CDe), retrievals from geostationary orbit Himawari-8/AHI measurements can be evaluated properly. Furthermore, the atmospheric thermodynamic state from in situ sounding profiles can estimate the CTT and moisture when radiosonde is effectively collocated with cloud geographical location and associated CTH in 3-D geometry. These data could help quantify the uncertainty of Himawari-8/AHI cloud retrievals comprehensively.

The 5-day intercomparison between AHI and Aqua/MODIS cloud products during the unstable atmospheric condition in the EASMO period over the SCS is presented. Mean statistics show that reasonable CTHs are generally obtained from AHI and MODIS. Inconsistencies between AHI and MODIS CTH might be due to the limited spectral observation of AHI in the CO<sub>2</sub> absorption region. Thus, the ability to retrieve optically

thin cirrus has relatively high uncertainties. However, AHI still provides cloud retrievals continuously due to its geostationary location. In addition, both AHI and MODIS have similar COT and CDe retrievals; however, AHI has slightly larger values. Further evaluation with CloudSat/CPR and CALIPSO/CALIOP confirmed that both AHI and MODIS mirror CPR cloud top; however, MODIS covers higher cloud-top altitude probably due to its advantageous spatial resolution. Therefore, the effective cloud-top retrieval is higher with MODIS than with AHI when double layers of clouds are present. This might influence both COT and cloud particle size retrievals because of the limitation of 1DVAR technique.

The independent evaluation of CTH and CTT using in situ radiosondes during two RV cruises in SCSTIMX over the SCS support the retrieval of AHI clouds. The spatiotemporal collocation, by considering of AHI's

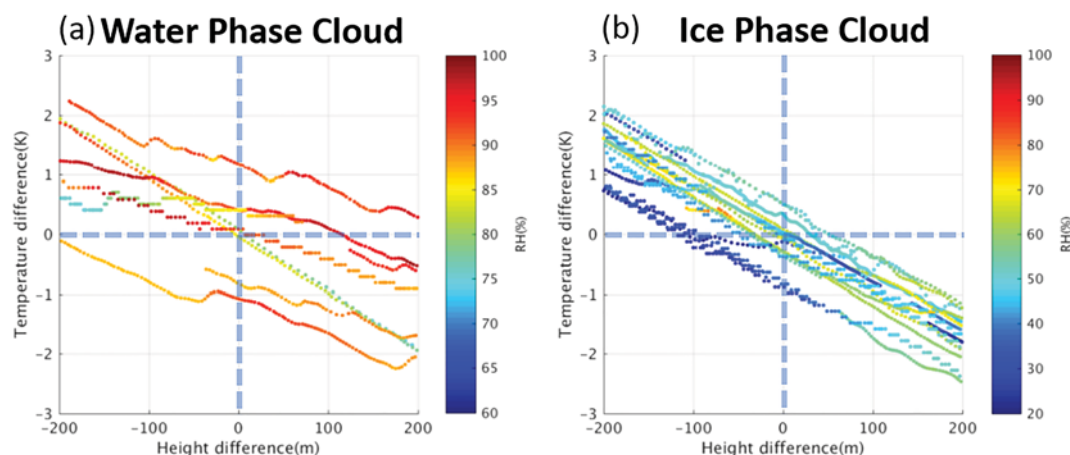


**Figure 7.** The temperature difference from CTT (y axis) and collocated CTH (x axis). The zero at y axis is considered the perfect match of radiosonde temperature at CTT. The positive (negative) values of x axis correspond to the altitude below (above) the altitude of cloud top. The color shading of each dot in the panel is the RH. Panel (a) presents the analysis of water phase clouds, and panel (b) presents the analysis of ice phase clouds.



scan time and radiosondes' geolocation in 3-D geometry, ensures the radiosonde could probe the cloud-top thermodynamic state. The result shows that AHI CTH retrievals are within 170 m from the cloud-top altitudes which are determined by using the radiosondes' temperature and moisture (i.e., RH) profiles as reference.

Because the cloudy radiance is a nonlinear function of the atmospheric and cloud parameters, multichannel or high-spectral resolution observation is expected to provide good cloud retrievals. MODIS has spectral observation of 13.4–15  $\mu\text{m}$ , which is crucial for upper tropospheric and lower stratospheric clouds. Cloud retrievals with synergistic use of multiple sensors (Liu et al., 2008, 2014; Liu, Li, et al., 2016) may be better than with using either one of them individually. Additional observation, such as aircraft, will help to quantify and ensure the estimated cloud microphysical properties in future, which might benefit the satellite precipitation product estimates as well (e.g., Liu et al., 2020). New retrieval techniques such as machine learning that can avoid large uncertainty of radiative transfer model in cloudy skies (Li et al., 2017) and well handle the nonlinearity between IR radiances and cloud properties, can be used for improving the cloud-top product through combining both active and passive remote sensing measurements (Min et al., 2020). Placing an advanced IR sounder onboard the geostationary platform (Schmit et al., 2009) would also enhance the cloud-top property retrievals when used together with measurements from the advanced imager onboard the same platform, such as the cloud clearing on polar-orbiting satellite (Li, Huang, et al., 2005) could be conducted at current Feng-Yun-4A.

## Data Availability Statement

MODIS data were obtained from the NASA Goddard Distributed Active Archive Center (DAAC) data archive. CALIOP data were obtained from the NASA the Atmospheric Science Data Center (ASDC). MODIS and CALIOP data used are listed in the references or archived online (<https://ladsweb.modaps.eos-dis.nasa.gov/search/repository>). CloudSat data are freely available via the CloudSat Data Processing Center (<http://www.cloudsat.cira.colostate.edu/>).

## Acknowledgments

This work is support by Ministry of Science and Technology of Taiwan (Grants MOST108-2625-M-008-015, MOST106-2111-M-008-001-MY2, and MOST105-2923-M-008-001-MY3). Chi-Hao Chiu was supported in part by Academic Sinica (Grant AS-TP-107-M10-3). The authors greatly appreciate the thoughtful comments and suggestions of Dr. Martin Setvák along with other two anonymous reviewers.

## References

- Ackerman, S. A., Moeller, C. C., Strabala, K. I., Gerber, H. E., Gumley, L. E., Menzel, W. P., & Tsay, S. C. (1998). Retrieval of effective microphysical properties of clouds: A wave cloud case study. *Geophysical Research Letters*, 25(8), 1121–1124. <https://doi.org/10.1029/98GL00042>
- Bayler, G. M., Aune, R. M., & Raymond, W. H. (2000). NWP cloud initialization using GOES sounder data and improved modeling of nonprecipitating clouds. *Monthly Weather Review*, 128(11), 3911–3920. [https://doi.org/10.1175/1520-0493\(2001\)129<3911:NCIUGS>2.0.CO;2](https://doi.org/10.1175/1520-0493(2001)129<3911:NCIUGS>2.0.CO;2)
- Bedka, K. M., Wang, C., Rogers, R., Carey, L. D., Feltz, W., & Kanak, J. (2015). Examining deep convective cloud evolution using total lightning, WSR-88D, and GOES-14 super rapid scan datasets. *Weather and Forecasting*, 30(3), 571–590. <https://doi.org/10.1175/WAF-D-14-00062.1>
- Bessho, K., Date, K., Hayashi, M., Ikeda, A., Imai, T., Inoue, H., et al. (2016). An introduction to Himawari-8/9—Japan's new-generation geostationary meteorological satellites. *Journal of the Meteorological Society of Japan. Ser. II*, 94(2), 151–183. <https://doi.org/10.2151/jmsj.2016-009>
- Coakley, J. A. Jr., & Bretherton, F. P. (1982). Cloud cover from high-resolution scanner data: Detecting and allowing for partially filled fields of view. *Journal of Geophysical Research*, 87(C7), 4917–4932. <https://doi.org/10.1029/JC087iC07p04917>
- Diaz, J. P., González, A., Expósito, F. J., Pérez, J. C., Fernández, J., García-Díez, M., & Taima, D. (2015). WRF multi-physics simulation of clouds in the African region. *Quarterly Journal of the Royal Meteorological Society*, 141(692), 2737–2749. <https://doi.org/10.1002/qj.2560>
- Eyre, J. R., & Woolf, H. M. (1988). Transmittance of atmospheric gases in the microwave region: A fast model. *Applied Optics*, 27(15), 3244–3249. <https://doi.org/10.1364/AO.27.003244>
- Greenwald, T. J., Pierce, R. B., Schaack, T., Otkin, J., Rogal, M., Bah, K., et al. (2016). Real-time simulation of the GOES-R ABI for user readiness and product evaluation. *Bulletin of the American Meteorological Society*, 97(2), 245–261. <https://doi.org/10.1175/BAMS-D-14-00007.1>
- Hamada, A., & Takayabu, Y. N. (2016). Convective cloud top vertical velocity estimated from geostationary satellite rapid-scan measurements. *Geophysical Research Letters*, 43, 5435–5441. <https://doi.org/10.1002/2016GL068962>
- Heidinger, A. K., Evan, A. T., Foster, M. J., & Walther, A. (2012). A naive Bayesian cloud-detection scheme derived from CALIPSO and applied within PATMOS-x. *Journal of Applied Meteorology and Climatology*, 51(6), 1129–1144. <https://doi.org/10.1175/JAMC-D-11-02.1>
- Huo, J., Lu, D., Duan, S., Bi, Y., & Liu, B. (2020). Comparison of the cloud top heights retrieved from MODIS and AHI satellite data with ground-based Ka-band radar. *Atmospheric Measurement Techniques*, 13(1), 1–11. <https://doi.org/10.5194/amt-13-1-2020>
- King, M. D., Kaufman, Y. J., Menzel, W. P., & Tanré, D. (1992). Remote sensing of cloud, aerosol, and water vapor properties from the Moderate Resolution Imaging Spectrometer (MODIS). *IEEE Transactions on Geoscience and Remote Sensing*, 30(1), 2–27. <https://doi.org/10.1109/36.124212>
- Kobayashi, T., & Masuda, K. (2008). Effects of precipitation on the relationships between cloud optical thickness and drop size derived from space-borne measurements. *Geophysical Research Letters*, 35, L24809. <https://doi.org/10.1029/2008GL036140>
- Korolev, A., & Isaac, G. A. (2006). Relative humidity in liquid, mixed-phase, and ice clouds. *Journal of the Atmospheric Sciences*, 63(11), 2865–2880. <https://doi.org/10.1175/JAS3784.1>

- Lai, R., Teng, S., Yi, B., Letu, H., Min, M., Tang, S., & Liu, C. (2019). Comparison of cloud properties from Himawari-8 and FengYun-4A geostationary satellite radiometers with MODIS cloud retrievals. *Remote Sensing*, 11(14), 1703. <https://doi.org/10.3390/rs11141703>
- Letu, H., Nagao, T. M., Nakajima, T. Y., Riedi, J., Ishimoto, H., Baran, A. J., et al. (2019). Ice cloud properties from Himawari-8/AHI next-generation geostationary satellite: Capability of the AHI to monitor the DC cloud generation process. *IEEE Transactions on Geoscience and Remote Sensing*, 57(6), 3229–3239. <https://doi.org/10.1109/TGRS.2018.2882803>
- Li, J., Huang, H.-L., Liu, C.-Y., Yang, P., Schmit, T. J., Wei, H., et al. (2005). Retrieval of cloud microphysical properties from MODIS and AIRS. *Journal of Applied Meteorology*, 44(10), 1526–1543. <https://doi.org/10.1175/JAM2281.1>
- Li, J., Liu, C.-Y., Huang, H.-L., Schmit, T. J., Wu, X., Menzel, W. P., & Gurka, J. J. (2005). Optimal cloud-clearing for AIRS radiances using MODIS. *IEEE Transactions on Geoscience and Remote Sensing*, 43(6), 1266–1278. <https://doi.org/10.1109/TGRS.2005.847795>
- Li, J., Menzel, W. P., & Schreiner, A. J. (2001). Variational retrieval of cloud parameters from goes sounder longwave cloudy radiance measurements. *Journal of Applied Meteorology*, 40(3), 312–330. [https://doi.org/10.1175/1520-0450\(2001\)040<0312:VROCPF>2.0.CO;2](https://doi.org/10.1175/1520-0450(2001)040<0312:VROCPF>2.0.CO;2)
- Li, J., Li, Z., Wang, P., Schmit, T. J., Bai, W., & Atlas, R. (2017). An efficient radiative transfer model for hyperspectral IR radiance simulation and applications under cloudy-sky conditions. *Journal of Geophysical Research: Atmospheres*, 122, 7600–7613. <https://doi.org/10.1002/2016JD026273>
- Liu, C.-Y., Aryastana, P., Liu, G.-R., & Huang, W.-R. (2020). Assessment of satellite precipitation product estimates over Bali Island. *Atmospheric Research*, 244, 105032. <https://doi.org/10.1016/j.atmosres.2020.105032>
- Liu, C.-Y., Kuo, S.-C., Lim, A. H. N., Hsu, S.-C., Tseng, K.-H., Yeh, N.-C., & Yang, Y.-C. (2016). Optimal use of space-borne advanced infrared and microwave soundings for regional numerical weather prediction. *Remote Sensing*, 8(10), 816. <https://doi.org/10.3390/rs8100816>
- Liu, C.-Y., Li, J., Ho, S. P., Liu, G. R., Lin, T. H., & Young, C. C. (2016). Retrieval of atmospheric thermodynamic state from synergistic use of radio occultation and hyperspectral infrared radiances observations. *IEEE Journal of Selected Topics in Applied Earth Observations and Remote Sensing*, 9(2), 744–756. <https://doi.org/10.1109/JSTARS.2015.2444274>
- Liu, C.-Y., Li, J., Weisz, E., Schmit, T. J., Ackerman, S. A., & Huang, H. L. (2008). Synergistic use of AIRS and MODIS radiance measurements for atmospheric profiling. *Geophysical Research Letters*, 35, L21802. <https://doi.org/10.1029/2008GL035859>
- Liu, C.-Y., Liu, G. R., Lin, T. H., Liu, C. C., Ren, H., & Young, C. C. (2014). Using surface stations to improve sounding retrievals from hyperspectral infrared instruments. *IEEE Transactions on Geoscience and Remote Sensing*, 52(11), 6957–6963. <https://doi.org/10.1109/TGRS.2014.2305992>
- Liu, Y., Key, J. R., Ackerman, S. A., Mace, G. G., & Zhang, Q. (2012). Arctic cloud macrophysical characteristics from CloudSat and CALIPSO. *Remote Sensing of Environment*, 124, 159–173. <https://doi.org/10.1016/j.rse.2012.05.006>
- Martin, G. (2007). *GEOCAT manual: GEOCAT version 0.5* (pp. 1–30). Cooperative Institute for Meteorological Satellite Studies, University of Wisconsin–Madison. Retrieved from [ftp://ftp.ssec.wisc.edu/pub/geocat/old/version\\_0\\_5/geocat\\_manual\\_v0\\_5.pdf](ftp://ftp.ssec.wisc.edu/pub/geocat/old/version_0_5/geocat_manual_v0_5.pdf)
- Martin, G., Gumley, L., Bearson, N., Braun, J., Cureton, G., Garcia, R., et al. (2016). *Support for GOES-R and Himawari-8 in CSPP Geo*. Retrieved from [http://cimss.ssec.wisc.edu/csppgeo/includes/documents/AMS2016\\_GMartin\\_CSPP\\_Geo.pdf](http://cimss.ssec.wisc.edu/csppgeo/includes/documents/AMS2016_GMartin_CSPP_Geo.pdf) (Accessed 31 January 2020).
- Menzel, P. W., Frey, R. A., Zhang, H., Wylie, D. P., Moeller, C. C., Holz, R. E., et al. (2008). MODIS global cloud-top pressure and amount estimation: Algorithm description and results. *Journal of Applied Meteorology and Climatology*, 47(4), 1175–1198. <https://doi.org/10.1175/2007JAMC1705.1>
- Menzel, W. P., Frey, R. A., Borbas, E. E., Baum, B. A., Cureton, G., & Bearson, N. (2016). Reprocessing of HIRS satellite measurements from 1980 to 2015: Development toward a consistent decadal cloud record. *Journal of Applied Meteorology and Climatology*, 55(11), 2397–2410. <https://doi.org/10.1175/JAMC-D-16-0129.1>
- Min, M., Li, J., Wang, F., Liu, Z., & Menzel, W. P. (2020). Retrieval of cloud top properties from advanced geostationary satellite imager measurements based on machine learning algorithms. *Remote Sensing of Environment*, 239, 111616. <https://doi.org/10.1016/j.rse.2019.111616>
- Molnar, G., & Coakley, J. A. Jr. (1985). Retrieval of cloud cover from satellite imagery data: A statistical approach. *Journal of Geophysical Research*, 90(D7), 12,960–12,970. <https://doi.org/10.1029/JD090iD07p12960>
- Platnick, S., King, M. D., Ackerman, S. A., Menzel, W. P., Baum, B. A., Riédi, J. C., & Frey, R. A. (2003). The MODIS cloud products: Algorithms and examples from terra. *IEEE Transactions on Geoscience and Remote Sensing*, 41(2 PART 1), 459–472. <https://doi.org/10.1109/TGRS.2002.808301>
- Schmit, T. J., Gunshor, M. M., Menzel, W. P., Gurka, J. J., Li, J., & Bachmeier, A. S. (2005). Introducing the next-generation advanced baseline imager on GOES-R. *Bulletin of the American Meteorological Society*, 86(8), 1079–1096. <https://doi.org/10.1175/BAMS-86-8-1079>
- Schmit, T. J., Li, J., Ackerman, S. A., & Gurka, J. J. (2009). High-spectral- and high-temporal-resolution infrared measurements from geostationary orbit. *Journal of Atmospheric and Oceanic Technology*, 26(11), 2273–2292. <https://doi.org/10.1175/2009JTECHA1248.1>
- Sohn, B. J., Choi, M. J., & Ryu, J. (2015). Explaining darker deep convective clouds over the western Pacific than over tropical continental convective regions. *Atmospheric Measurement Techniques*, 8(11), 4573–4585. <https://doi.org/10.5194/amt-8-4573-2015>
- Stephens, G. L., Tsay, S. C., Stackhouse, P. W., & Flatau, P. J. (1990). The relevance of the microphysical and radiative properties of cirrus clouds to climate and climatic feedback. *Journal of the Atmospheric Sciences*, 47(14), 1742–1754. [https://doi.org/10.1175/1520-0469\(1990\)047<1742:trotma>2.0.co;2](https://doi.org/10.1175/1520-0469(1990)047<1742:trotma>2.0.co;2)
- Stephens, G. L., Vane, D. G., Tanelli, S., Im, E., Durden, S., Rokey, M., et al. (2009). CloudSat mission: Performance and early science after the first year of operation. *Journal of Geophysical Research*, 113, D00A18. <https://doi.org/10.1029/2008JD009982>
- Strabala, K. I., Ackerman, S. A., & Menzel, W. P. (1994). Cloud properties inferred from 8–12- $\mu$ m data. *Journal of Applied Meteorology*, 33(2), 212–229. [https://doi.org/10.1175/1520-0450\(1994\)033<0212:CPIFD>2.0.CO;2](https://doi.org/10.1175/1520-0450(1994)033<0212:CPIFD>2.0.CO;2)
- Sui, C.-H., Lin, P.-H., Chen, W.-T., Jan, S., Liu, C.-Y., Yang, Y. J., et al. (2020). The South China Sea Two Islands Monsoon Experiment for studying convection and subseasonal to seasonal variability. *Terrestrial, Atmospheric and Oceanic Sciences*, 31(2), 103–129. <https://doi.org/10.3319/tao.2019.11.29.02>
- Tan, Z., Ma, S., Zhao, X., Yan, W., & Lu, W. (2019). Evaluation of cloud top height retrievals from China's next-generation geostationary meteorological satellite FY-4A. *Journal of Meteorological Research*, 33(3), 553–562. <https://doi.org/10.1007/s13351-019-8123-0>
- Várnai, T., & Marshak, A. (2007). View angle dependence of cloud optical thicknesses retrieved by Moderate Resolution Imaging Spectroradiometer (MODIS). *Journal of Geophysical Research*, 112, D06203. <https://doi.org/10.1029/2005JD006912>
- Wang, B., LinHo, Z., & Lu, M. M. (2004). Definition of South China Sea monsoon onset and commencement of the East Asian summer monsoon. *Journal of Climate*, 17(4), 699–710. <https://doi.org/10.1175/2932.1>

- Wang, T., Fetzer, E. J., Wong, S., Kahn, B. H., & Yue, Q. (2016). Validation of MODIS cloud mask and multilayer flag using CloudSat-CALIPSO cloud profiles and a cross-reference of their cloud classifications. *Journal of Geophysical Research*, *121*, 11,620–11,635. <https://doi.org/10.1002/2016JD025239>
- Weisz, E., Li, J., Menzel, W. P., Heidinger, A. K., Kahn, B. H., & Liu, C.-Y. (2007). Comparison of AIRS, MODIS, CloudSat and CALIPSO cloud top height retrievals. *Geophysical Research Letters*, *34*, L17811. <https://doi.org/10.1029/2007GL030676>
- Winker, D. M., Hunt, W. H., & McGill, M. J. (2007). Initial performance assessment of CALIOP. *Geophysical Research Letters*, *34*, L19803. <https://doi.org/10.1029/2007GL030135>
- Yao, Z., Li, J., Weisz, E., Heidinger, A., & Liu, C. Y. (2013). Evaluation of single field-of-view cloud top height retrievals from hyperspectral infrared sounder radiances with CloudSat and CALIPSO measurements. *Journal of Geophysical Research: Atmospheres*, *118*, 9182–9190. <https://doi.org/10.1002/jgrd.50681>